Iranian J. Math. Chem. 8 (4) December (2017) 345 − 364

Iranian Journal of Mathematical Chemistry

Journal homepage: ijmc.kashanu.ac.ir

A Numerical Study of Fractional Order Reverse Osmosis Desalination Model using Legendre Wavelet Approximation

OMAR BELHAMITI[1,•] AND BELKACEM ABSAR[2]

[1]Laboratory of Pure and Applied Mathematics, Abdelhamid Ibn Badis University, Mostaganem 27000, Algeria

[2]Laboratory of Science and Technology of the Environment and Promotion, University of Mostaganem, Mostaganem 27000, Algeria

ARTICLE INFO

Article History:

Received: 20 May, 2017
Accepted: 8 June 2017
Published online 6 July 2017
Academic Editor: Ivan Gutman

Keywords:

Reverse osmosis desalination system
Legendre wavelet method
DQL- technique
Caputo fractional derivative

ABSTRACT

The purpose of this study is to develop a new approach in modeling and simulation of a reverse osmosis desalination system by using fractional differential equations. Using the Legendre wavelet method combined with the decoupling and quasi-linearization technique, we demonstrate the validity and applicability of our model. Examples are developed to illustrate the fractional differential technique and to highlight the broad applicability and the efficiency of this method. The fractional derivative is described in the Caputo sense.

1. INTRODUCTION

In recent few decades, fractional calculus has caught much attention due to its ability to provide an accurate description of different nonlinear phenomena. Moreover, the fractional differential equations have gained considerable popularity of many researchers due to their applications in many engineering and scientific disciplines such as control theory, signal processing, information sciences, and many other physical and chemical processes and also in medical sciences, see [15−18, 20, 21, 24]. These equations are also used in the modeling

• Corresponding Author: (Email address: (omar.belhamiti@univ-mosta.dz)
DOI: 10.22052/ijmc.2017.86494.1289

of physical processes running in dynamic mode [23, 22]. In this way, this work deals with the application of fractional derivatives for the desalination phenomenon.

On the other hand, desalination of sea water appears as a strategic solution adopted by several countries to cope with drinking water availability problem. This process was intended only for industrial purposes due to the constraints of high desalination costs [1−5]. However, technological advances in the field of manufacture of membranes have reduced these costs and thus enable more countries to use this alternative as a freshwater resource. Actually, re-verse osmosis, due to its lower energy consumption and simplicity has gained much wider acceptance than the thermal alternatives. Reverse osmosis is based on a physical property called semi-permeability. Certain polymeric materials (membranes) allow water to pass more quickly than some substances such as dissolved salts. The principle is to apply a high enough pressure to overcome the osmotic pressure and reverse the flow of water.

Many mathematical models have been proposed to describe the performance of reverse osmosis unit. For more details, we cite [1−5]. But, since the memory of phenomena plays a key role in mechanics, so a possible generalization of the classic desalination model would be a system with fractional order derivative. In this line of thought, Du et al. [11] found that a physical meaning of the fractional order is an index of memory. Then, Atangana et al. [8] proved that a fractional operator can provide a better interpretation of both physical and engineering processes.

The authors in [30, 31] studied the overall performance of hollow fiber membranes by using the interplay of fiber productivity (defined as the fraction of feed recovered as permeate) and fiber selectivity or rejection. Two flow configuration modules for reverse osmosis hollow fiber membranes are considered: co-current and counter-current flow. Productivity and selectivity were plotted as functions of fiber length. It is found that at the entrance of the module, the term of productivity is equal to zero. This trend (flattening of the curve of productivity) is observed in the neighborhood of the entrance to the tube for the two cases: Co-current and Cross-current. This phenomenon is explained by the fact that the feed rate is constant and therefore the first derivative is equal to zero.

In this paper, we will focus on the use of the fractional differential operator in the sense of Caputo for modeling a seawater desalination module using the reverse osmosis process. The numerical solution of the fractional differential model (FDM) is obtained by using the Legendre wavelet method combined with the decoupling and quasi-linearization technique. For more information about this new approach, we refer the reader to [6,7,9,14]. In this approach the Block-Pulse functions (BPFs) and the operational matrix of integration are used, FDM can be transformed to lower triangular system of algebraic equations. Then the solution of this system is used to determine a new numerical solution of FDM. At the end, and since the approach is not yet tested sufficiently on FDEs, some other problems are studied.

This work is organized as follows: Section 2 gives the fundamental equations to describe the transport phenomena in reverse osmosis by using the fractional model. Section 3 introduces some necessary definitions of the Legendre wavelet method. We present a new operational fractional matrix of integration and we give the description of the proposed method. Section 4 gives the numerical investigations of the analytical findings. At the end, a conclusion follows.

2. MODELING OF REVERSE OSMOSIS DESALINATION SYSTEM

2.1. CLASSICAL MODEL OF REVERSE OSMOSIS DESALINATION SYSTEM

Sea water desalination has become an inevitable alternative for many countries to overcome the shortage of natural fresh water. Among desalination technology, reverse osmosis is the most used method. This is mainly due to its simplicity, their costs, reduced compared to thermal processes. No heating or phase separation change is necessary. The major energy required for desalting is for pressurizing the seawater feed [19]. Reverse osmosis is a method of separation and concentration in the liquid phase. This process is applied to purify water for laboratory. The process consists in passing aqueous solution under pressure through an appropriate membrane and withdrawing the membrane permeate at atmospheric pressure and ambient temperature. The product obtained is enriched in one of the mixture components. The other components are recovered in the retentate with higher concentration in the high-pressure side of the membrane. Reverse osmosis membranes are generally mounted on supports called modules. Currently, the most used modules are: hollow fiber, tubular and spiral wound modules. Tubular modules are constituted of two concentric tubes designed to separate a given feed into a higher pressure stream (retentate) and a low pressure stream (permeate) see figure 1. According to the direction of the feed flow rate, there are two types of flow pattern: the co-current and counter-current flow pattern.

Figure 1: Hollow fiber membrane.

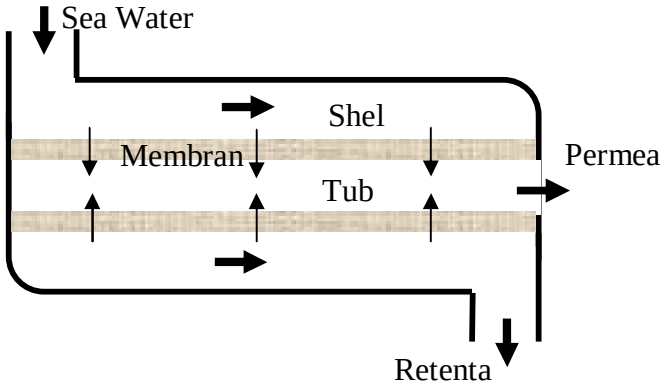

A mathematical model was developed to predict the performance of hollow fiber reverse osmosis membrane with co-current flow pattern. The mass transfer model employed in this study is the solution-diffusion model. The solvent and salt mass flux are expressed by Fick's law. This model is developed by the author [1, 2]. It consists of a set of four strongly nonlinear differential equations. This system is found, according to material balance principle:

$$\begin{cases} \frac{dQ_{sw}}{dx} = -\pi \frac{A_w}{\sigma_w} D_m \left(\Delta P - \kappa \left(\frac{\dot{Q}_{ss}}{Q_{sw}} - \frac{\dot{Q}_{fs}}{Q_{fw}} \right) \right) \\ \frac{dQ_{fw}}{dx} = \pi \frac{A_w}{\sigma_w} D_m \left(\Delta P - \kappa \left(\frac{\dot{Q}_{ss}}{Q_{sw}} - \frac{\dot{Q}_{fs}}{Q_{fw}} \right) \right) \\ \frac{d\dot{Q}_{ss}}{dx} = -\pi B_s D_m \left(\frac{\dot{Q}_{ss}}{Q_{sw}} - \frac{\dot{Q}_{fs}}{Q_{fw}} \right) \\ \frac{d\dot{Q}_{fs}}{dx} = \pi B_s D_m \left(\frac{\dot{Q}_{ss}}{Q_{sw}} - \frac{\dot{Q}_{fs}}{Q_{fw}} \right), \end{cases} \quad (1)$$

where

Q_{sw} : is the water volumetric flow rate in the shell side,

Q_{fw} : is the water volumetric flow rate in the fiber side,

$\dot{Q}_{ss}$: represents the solute mass flow rate in the shell side,

$\dot{Q}_{ss}$: is the solute mass flow rate in the fiber side,

κ is a proportionality coefficient,

A_w is the water permeability coefficient (a function of salt diffusivity through the membrane),

ΔP is the transmembrane pressure (a function of the feed, concentrate and permeate concentrations),

σ_w is the water density,

B_s is the solute permeability coefficient,

The osmotic pressure is approximately represented by a linear function of solute concentrations $\pi = \kappa C$.

2.2. REVERSE OSMOSIS DESALINATION MODEL

Lately, it has frequently been observed that the mathematical models represented by fractional order derivatives [11, 12, 13, 20] can provide better agreement between measured and simulated data than classical models based on integer order derivatives. In

classical desalination model [1, 2, 7], instead of a variation of order one, we consider, in this study, a variation of the order $1 < \alpha < 2$. Taking into account normalized variables,

$$\boldsymbol{Q}_{sw} = \frac{Q_{sw}}{Q_{sw0}}, \boldsymbol{Q}_{fw} = \frac{Q_{fw}}{Q_{sw0}}, \dot{\boldsymbol{Q}}_{ss} = \frac{\dot{Q}_{ss}}{\dot{Q}_{ss0}}, \dot{\boldsymbol{Q}}_{fs} = \frac{\dot{Q}_{fs}}{\dot{Q}_{ss0}},$$

if we replace the first order derivatives by fractional derivatives in (1), then a simple dimensional analysis shows that the left-hand sides of the equations have the dimension of $(\text{space})^{-\alpha}$. But an examination of the right-hand sides shows that they have the dimension of $(\text{space})^{-1}$, so, we need to modify the right-hand sides to adjust the dimensions [12]. Thus, we formulate the fractional model of reverse osmosis desalination using Caputo fractional derivatives of order, $1 < \alpha < 2$ [10], the model is described by the non-linear Caputo fractional differential system:

$$\begin{cases} {}_0D_x^{\alpha} Q_{sw} = -c_1 + c_2 \left(\frac{\dot{Q}_{ss}}{Q_{sw}} - \frac{\dot{Q}_{fs}}{Q_{fw}} \right) \\ {}_0D_x^{\alpha} Q_{fw} = c_1 - c_2 \left(\frac{\dot{Q}_{ss}}{Q_{sw}} - \frac{\dot{Q}_{fs}}{Q_{fw}} \right) \\ {}_0D_x^{\alpha} Q_{fw} = -c_3 \left(\frac{\dot{Q}_{ss}}{Q_{sw}} - \frac{\dot{Q}_{fs}}{Q_{fw}} \right) \\ {}_0D_x^{\alpha} Q_{fw} = c_3 \left(\frac{\dot{Q}_{ss}}{Q_{sw}} - \frac{\dot{Q}_{fs}}{Q_{fw}} \right), \end{cases} \tag{2}$$

where

$$c_1 = \left(\pi \frac{A_w}{\sigma_w} \frac{D_m}{Q_{sw0}} \Delta P \right)^{\alpha}$$
$$c_2 = \left(\pi \frac{A_w}{\sigma_w} \frac{D_m}{Q_{sw0}} \frac{\dot{Q}_{ss}}{Q_{sw0}} \right)^{\alpha}$$
$$c_3 = \left(\pi B_s \frac{D_m}{Q_{sw0}} \right)^{\alpha}.$$

Note that in the limit case $\alpha \to 1$, the system (2) reduces to the classical system (1).

3. LEGENDRE WAVELET METHOD

In this section, we present some definitions and properties of fractional calculus. Then, we introduce some preliminaries on Legendre wavelets that are used throughout this paper. This section is ended by presenting some definitions, notations and basic facts of block pulse functions, [25–27].

Let $(n-1) \leq \alpha < n, n \in \mathbb{N}^*$, a function $f \in C^n\ (a,b)$. The Caputo derivative of order $\alpha \geq 0$ is defined by

$$
\begin{aligned}
{}_0^C D_t^\alpha f(t) &= \frac{1}{\Gamma(n-\alpha)} \int_\alpha^t (t-\tau)^{n-\alpha-1} f^{(n)}(\tau)\, d\tau \\
&= I_t^{n-\alpha} \left(\frac{d^n}{dt^n} f(t) \right),
\end{aligned}
$$

where

$$
\Gamma(\alpha) := \int_0^\infty e^{-u}\, u^{\alpha-1} du, \quad Re\{\alpha\} > 0
$$

We note that the Caputo derivative of a constant function is zero. For more details on fractional calculus, we refer the reader to [10, 13].

3.1. LEGENDRE WAVELETS

On the other hand, the wavelets are a family of functions constructed from dilatations and translations of a single function called the mother wavelet. We have the following family of continuous wavelets

$$
\psi_{a,b}(t) = |a|^{-\frac{1}{2}} \psi\left(\frac{t-b}{a}\right), a, b\ \mathbb{R}, a \neq 0,
$$

where $\psi(t) \in L^2(\mathbb{R})$, a and b represent the dilation and the translation parameters respectively. If a and b have discrete values as

$$
\begin{cases} a = a_0^{-k}, a_0 > 1 \\ b = n\, b_0\, a_0^{-k}, b_0 > 1 \end{cases} \qquad n, k \in \mathbb{N},
$$

for n and m positive integers, we have the following family of discrete wavelets:

$$
\psi_{m,n}(t) = |a_0|^{\frac{m}{2}} \psi(a_0^m t - n\, b_0)
$$

where $\psi_{m,n}(t)$ forms a wavelet basis for $L^2(\mathbb{R})$. In particular, when $a_0 = 2$ and $b_0 = 1$, $\psi_{m,n}(t)$ forms an orthonormal basis. That is $\langle \psi_{m,n}, \psi_{l,k} \rangle = \delta_{m,l}\, \delta_{n,k}$ in which $\langle .,. \rangle$ denotes the inner product in $L^2([0,1])$.

In this work, the mother wavelet is the Legendre polynomials. We de ne the orthogonal Legendre polynomials of order m by the following Rodriguez recurrence formula:

$$\begin{cases} L_0(t) = 1 \\ L_1(t) = t \\ L_{m+2}(t) = \left(\frac{2\,m+3}{m+2}\right) t\, L_{m+1}(t) - \left(\frac{m+1}{m+2}\right) L_m(t), \end{cases}$$

with $m = 0,1,2,3,\ldots$ and t varies into [-1,1].

The Legendre wavelets are defined in [0; 1] by the following formula

$$\psi_{m,n}(t) = \begin{cases} \sqrt{m + 1/2}\, 2^{\frac{1}{2}}\, L_m\left(2^j t - 2n + 1\right) & \text{if } \frac{n-1}{2^{j-1}} \le t \le \frac{n}{2^{j-1}} \\ 0, & \text{otherwise,} \end{cases}$$

where $n = 1, \ldots, 2^{j-1}$ $(j \in \mathbb{N} \setminus \{0\})$, $m = 0, \ldots, n_c - 1$ $(n_c \in \mathbb{N} \setminus \{0\})$ is the order of the Legendre polynomials and *nc* is the number of collocation points. However, the dilatation parameter is $a = 2^{j/2}$ and the translation parameter is $b = (2n-1)2^{j/2}$.

The family

$$\{\psi_{m,n}(t)\}_{\substack{n=1,\ldots,2^{j-1} \\ m=0,\ldots,nc-1}}$$

forms an orthonormal basis of $L^2([0,1])$ [26]. Then, any function $f \in L^2([0,1])$ may be decomposed as

$$f(t) = \sum_{n=1}^{+\infty} \sum_{m=0}^{+\infty} C_{n,m}\, \psi_{n,m}(t), \tag{3}$$

where $C_{n,m} = \langle f, \Psi \rangle$; in which $\langle .,. \rangle$ denoted the inner product in $L^2([0,1])$.

The function in (3) can be approached by

$$f(t) = \sum_{n=1}^{2^{j-1}} \sum_{m=0}^{nc-1} C_{n,m}\, \psi_{n,m}(t) = C^T\, \Psi(t), \tag{4}$$

where C and $\Psi(t)$ are $2^{j-1}\, nc$ vectors given by

$$C = \left[C_{1,0,\ldots,} C_{1,nc-1,} C_{2,0,\ldots,} C_{2,nc-1,\ldots,} C_{2^{j-1},1,\ldots,} C_{2^{j-1},nc-1}\right]^T \tag{5}$$

$$\Psi(t) = \left[\psi_{1,0}(t), \ldots, \psi_{1,nc-1}(t), \psi_{2,0}(t), \ldots, \psi_{2,nc-1}(t), \ldots, \psi_{2^{j-1},0}(t), \ldots, \psi_{2^{j-1},nc-1}(t)\right]^T \tag{6}$$

The following property of the product of two Legendre wavelet vector functions will also be used

$$A^T \Psi(t)\, \Psi^T(t) = \Psi^T(t)\, \bar{A}, \tag{7}$$

where

$$A = \left[a_{1,0}, \dots, a_{1,nc-1}, a_{2,0}, \dots, a_{2,nc-1}, \dots, \psi_{2^{j-1},0}(t), \dots, \psi_{2^{j-1},nc-1}(t)\right]^T$$

and $\bar{A}$ is a $2^{j-1}\,nc$x$2^{j-1}\,nc$ matrix [26].

3.2. BLOCK PULSE FUNCTION

The block functions form a complete set of orthogonal functions which can be defined over [0;T] by

$$b_i(t) = \begin{cases} 1, & \text{if } \frac{i-1}{2^{j-1}nc}T \le t < \frac{i}{2^{j-1}nc}\,T \\ 0, & \text{otherwise,} \end{cases} \tag{8}$$

where, $i = 1, \dots, 2^{j-1}nc$ [27]. There are some properties for block pulse functions: the most important properties are disjointness and orthogonality.

The disjointness property follows

$$b(t)\,b^T(t)\,V = \tilde{V}\,b(t)$$

and

$$\tilde{V} = \begin{pmatrix} V_1 & \cdots & 0 \\ \vdots & \ddots & \vdots \\ 0 & \cdots & V_{2^{j-1}\,nc} \end{pmatrix},$$

where V is an $2^{j-1}nc$-vector. The block-pulse functions are orthogonal

$$\int_0^T b_i(t),\ b_i(t)\,dt = \begin{cases} \frac{T}{2^{j-1}nc}, i = j \\ 0, \text{otherwise} \end{cases}$$

where *i; j* = 1, 2,…, $2^{j-1}nc$.

3.3. OPERATIONAL FRACTIONAL MATRIX OF INTEGRATION

In the following section, we introduce new arguments for deriving the fractional Legendre wavelets operational matrix of integration.

Let $t \in [0;\ 1]$ we define the Legendre wavelets operational matrix of integration as in [6, 26],

$$\int_0^t \Psi(x)\,dx = P\ \Psi(t), \tag{9}$$

where

$$P = \frac{1}{2^{j-1}} \begin{pmatrix} L & F & \cdots & F \\ 0 & L & \ddots & \vdots \\ \vdots & \ddots & \ddots & F \\ 0 & \cdots & 0 & L \end{pmatrix},$$

is the $2^{j-1}nc$ x $2^{j-1}nc$ operational matrix of integration, and L and F are nc x nc matrices. It is not difficult to see that

$$\left({}_0I_t^0\,\Psi\right)(t) = \Psi(t),$$

$$\left({}_0I_t^1\,\Psi\right)(t) = \int_0^t \Psi(x)\,dx = P\ \Psi(t),$$

$$\left({}_0I_t^2\,\Psi\right)(t) = \int_0^t \left(\int_0^s \Psi(x)\,dx\right) ds = \int_0^t P\Psi(s)\,ds = \mathrm{P\,x\,P\,x}\,\Psi(t) = \mathrm{P}^2\ \Psi(t),$$

$$\vdots$$

$$\left({}_0I_t^n\,\Psi\right)(t) = \int_0^t \left(\int_0^s \Psi(x)\,dx \left(\int_0^\tau \Psi(x)\,dx \ldots\right) ds\right) = \mathrm{P\,x\,P\,x} \ldots \mathrm{x}\,\Psi(t) = \mathrm{P}^n\ \Psi(t),$$

On the other hand, we have

$$\left({}_0I_t^n\,\Psi\right)(t) = \frac{1}{\Gamma(n)}\int_0^t (t-\tau)^{n-1}\Psi(\tau)\,d\tau, \qquad t \in [0,1].$$

Using the convolution product, we can write

$$\left({}_0I_t^n\,\Psi\right)(t) = (\Psi\,\mathrm{x}\,\phi)(t),$$

where

$$\phi(t) = \frac{(t-\tau)^{n-1}}{\Gamma(n)},\ \text{(a causal function)}.$$

The continuous character of the function Γ(α) is used to release Γ(n) and to define the integral operator of order α>0.This operator is defined as

$${}_0I_t^\alpha\,\Psi(t) = \begin{cases} \dfrac{1}{\Gamma(\alpha)}\displaystyle\int_0^t (t-\tau)^{\alpha-1}\Psi(\tau)\,d\tau, & \alpha > 0 \\ \Psi(t), & \alpha = 0, \end{cases}$$

so

$$\left({}_0I_t^\alpha\,\Psi\right)(t) = P^\alpha\Psi(t)\,,\ \alpha > 0. \tag{10}$$

Now, to define the fractional Legendre wavelets operational matrix of integration, we give a result, in the transition matrix of the base B to the base $\Psi(t)$.

Proposition 3.3.1. For m = 0,1,…, nc-1, the relation between the Legendre wavelet vector and m-set of block-pulse functions can be written as

$$\Psi(t) = H\,B(t), \tag{11}$$

where H is the $\left(2^{j-1}nc\right)$ x $\left(2^{j-1}nc\right)$ passage matrix

$$H = \begin{pmatrix} h_{1,0} & \cdots & h_{1,nc-1} & & & & & \\ \vdots & \ddots & \vdots & \cdots & & 0 & & \\ h_{nc,0} & \cdots & h_{nc,nc-1} & & & & & \\ & \vdots & & \ddots & & \vdots & & \\ & & & & h_{1,0} & \cdots & h_{1,nc-1} & \\ & 0 & & \cdots & \vdots & \ddots & \vdots & \\ & & & & h_{nc,0} & \cdots & h_{nc,nc-1} & \end{pmatrix},$$

and

$$h_{i,m} = \sqrt{2m+1}\ \sum_{k=0}^{m-1}(-1)^{m+k}\ \frac{(m+k)!}{(m-k)!\ (k!)^2\ nc^k}\ \frac{(i)^{k+1} - (i-1)^{k+1}}{(k+1)}$$

Proof. Let

$$h_{i,m} = \int_0^1 \Psi_{n,m}(t)\ b_i(t)\ dt = \sqrt{m+\frac{1}{2}}\ 2^{j/2}\ \int_{\frac{i-1}{q}}^{\frac{i}{q}} L_m\left(2^j t - 2\,n + 1\right)\ dt.$$

On the first level n = 1, this formula becomes

$$h_{i,m} = \sqrt{m+\tfrac{1}{2}}\ 2^{j/2}\ \int_{\frac{i-1}{q}}^{\frac{i}{q}} L_m\left(2^j t - 1\right)\ dt.$$

Assuming that $2^j t - 1$, we obtain

$$h_{i,m} = \sqrt{m+1/2}\ 2^{j/2}\ \int_{\frac{2i-2}{nc}-1}^{\frac{2i}{nc}-1} L_m\,(x)\ dx$$

$$= \sqrt{m+1/2}\,2^{j/2}\ \int_{\frac{2i-2}{nc}-1}^{\frac{2i}{nc}-1} \sum_{k=0}^{m-1}(-1)^{m+k}\binom{m}{k}\binom{m+k}{m}x^k dx$$

$$= \sqrt{m+1/2}\,2^{j/2}\ \sum_{k=0}^{m-1}(-1)^{m+k}\ \frac{(m+k)!}{(m-k)!\,(k!)^2\,nc^k\,q}\ \frac{(i)^{k+1} - (i-1)^{k+1}}{(k+1)},$$

We need also the following result [27]:

Proposition 3.3.2. Let $\alpha>0$. The fractional integral of block-pulse function vector can be written as

$$(I^{\alpha} B)(t) = F^{\alpha} B(t), \tag{12}$$

where F^{α} is the $(2^{j-1}nc)$ x $(2^{j-1}nc)$ matrix given by

$$F^{\alpha} = \left(\frac{T}{2^{j-1}nc}\right)^{\alpha} \frac{1}{\Gamma(\alpha+2)} \begin{pmatrix} f_1 & f_2 & f_3 & \cdots & f_{2^{j-1}nc} \\ & f_1 & f_2 & \cdots & f_{2^{j-1}nc-1} \\ & & f_1 & \cdots & f_{2^{j-1}nc-2} \\ & 0 & & \ddots & \vdots \\ & & & & f_1 \end{pmatrix},$$

and

$$\begin{cases} f_1 = 1, \\ f_p = p^{\alpha+1} - 2(p-1)^{\alpha+1} + (p-2)^{\alpha+1}, \qquad p = 2,3,\dots,2^{j-1}nc - i + 1, \end{cases}$$

with $i = 1,2,3,\dots,2^{j-1}nc$.

Now, we prove the following result for the fractional matrix of integration:

Theorem 3.3.3. The Legendre wavelets operational matrix P of fractional integration is given by

$$P^{\alpha} = H F^{\alpha} H^{-1}. \tag{13}$$

Proof. Using (10) and (11), we can write

$$\left({}_0I_t^{\alpha} \Psi\right)(t) = (I^{\alpha} H B)(t) = H(I^{\alpha} B)(t). \tag{14}$$

Thanks to (10) and (14), yields

$$P^{\alpha}\Psi(t) = HF^{\alpha} B(t). \tag{15}$$

By (11) and (15), we get

$$P^{\alpha} HB(t) = H F^{\alpha} B(t).$$

Therefore,

$$P^{\alpha} = H F^{\alpha-1}.$$

3.4. ILLUSTRATION OF THE APPROACH

In this subsection, we will describe our approach to solve numerically the system (2). We start with the decoupling and quasi-linearization iterative technique. It is summarized as follows:

Given initial profile for each solution: $\boldsymbol{Q}_{sw}^{(0)}(x), \boldsymbol{Q}_{fw}^{(0)}(x)\ , \dot{\boldsymbol{Q}}_{ss}^{(0)}(x), \dot{\boldsymbol{Q}}_{fs}^{(0)}(x)$

$$
\begin{aligned}
{}_0D_x^{\alpha}\boldsymbol{Q}_{sw}^{(k+1)} &= -c_1 + c_2\left(\frac{\dot{\boldsymbol{Q}}_{ss}^{(k+1)}}{\boldsymbol{Q}_{sw}^{(k+1)}} - \frac{\dot{\boldsymbol{Q}}_{fs}^{(k+1)}}{\boldsymbol{Q}_{fw}^{(k+1)}}\right)\\
{}_0D_x^{\alpha}\boldsymbol{Q}_{fw}^{(k+1)} &= c_1 - c_2\left(\frac{\dot{\boldsymbol{Q}}_{ss}^{(k+1)}}{\boldsymbol{Q}_{sw}^{(k+1)}} - \frac{\dot{\boldsymbol{Q}}_{fs}^{(k+1)}}{\boldsymbol{Q}_{fw}^{(k+1)}}\right)\\
{}_0D_x^{\alpha}Q_{fw} &= -c_3\left(\frac{\dot{\boldsymbol{Q}}_{ss}^{(k+1)}}{\boldsymbol{Q}_{sw}^{(k+1)}} - \frac{\dot{\boldsymbol{Q}}_{fs}^{(k+1)}}{\boldsymbol{Q}_{fw}^{(k+1)}}\right)\\
{}_0D_x^{\alpha}Q_{fw} &= c_3\left(\frac{\dot{\boldsymbol{Q}}_{ss}^{(k+1)}}{\boldsymbol{Q}_{sw}^{(k+1)}} - \frac{\dot{\boldsymbol{Q}}_{fs}^{(k+1)}}{\boldsymbol{Q}_{fw}^{(k+1)}}\right),
\end{aligned}
$$

where $U^{(k+1)}$ and $U^{(k)}$ are the approximations of the solution at the current and the preceding iteration, respectively.

To find a solution of (2), we apply the method described above for each equation and we calculate the decoupling and quasi-linearization error by using the following formula

$$E_{DQLT}^{(k+1)} = max\left(\left\|\boldsymbol{Q}_{sw}^{(k+1)} - \boldsymbol{Q}_{sw}^{(k)}\right\|_2, \left\|\boldsymbol{Q}_{fw}^{(k+1)} - \boldsymbol{Q}_{fw}^{(k)}\right\|_2, \dots, \left\|\dot{\boldsymbol{Q}}_{ss}^{(k+1)} - \dot{\boldsymbol{Q}}_{ss}^{(k)}\right\|_2\right) \quad (16)$$

where $\|\ .\ \|_2$ represents the Euclidian norm. This procedure gives the solution of the problem when the error is less than a given small epsilon.

For $u \in C^2([0,1])$, we develop our method for the problem

$$D^{\alpha}u(t) = g(t)\,u(t) + f(t), t \in]0,1], 0 < \alpha \leq 2 \quad (17)$$

such that

$$\begin{cases} u(0) = u_0 \\ u'(0) = u_1 \end{cases} \quad (18)$$

The condition $u'(0) = u_1$ is only for $1 < \alpha \leq 2$, where $f, g \in L^2([0,1])$. We approximate the derivative $D^{\alpha}u$ and the functions g and f as in (4) as follows :

$$\begin{cases} D^{\alpha}u(t) = U^T\Psi(t) \\ g(t) = G^T\Psi(t) \\ f(t) = F^T\Psi(t) \end{cases} \quad (19)$$

Using (10), we can write

$$\begin{aligned} u(t) &= I^{\alpha}\left(D^{\alpha}\, u(t)\right) + u(0) + u'(0)t \\ &= I^{\alpha}\left(U^{T}\,\Psi(t)\right) + u_0 d^{T}\,\Psi(t) + u_1 E^{T}\,\Psi(t) \\ &= U^{T} P^{\alpha}\,\Psi(t) + u_0 d^{T}\,\Psi(t) + u_1 E^{T}\,\Psi(t)\,, \end{aligned}$$

so

$$u(t) = \left(U^{T} P^{\alpha} + u_0 d^{T} + u_1 E^{T}\right)\Psi(t) \tag{20}$$

where $d = \langle 1, \Psi(t)\rangle_{L^2([0,1])}$ and $E = \langle t, \Psi(t)\rangle_{L^2([0,1])}$. Substituting (19) and (20) into (17), we have

$$U^{T}\Psi(t) = G^{T}\Psi(t)\left(U^{T} P^{\alpha} + u_0 d^{T} + u_1 E^{T}\right)\Psi(t) + F^{T}\,\Psi(t)$$

$$\Psi^{\mathrm{T}}(t)U = G^{T}\Psi(t)\Psi^{\mathrm{T}}(t)\left(U^{T} P^{\alpha} + u_0 d^{T} + u_1 E^{T}\right)^{T} + \Psi^{\mathrm{T}}(t)F$$

$$= \Psi^{\mathrm{T}}(t)\,\tilde{G}\left(U^{T} P^{\alpha} + u_0 d^{T} + u_1 E^{T}\right)^{T} + \Psi^{\mathrm{T}}(t)F$$

Thanks to (7), we obtain the following algebraic system

$$\left(I_d - \tilde{G}(P^{\alpha})^{T}\right) U = \tilde{G}(u_0 d^{T} + u_1 E^{T})^{T} + F. \tag{21}$$

The solution of the problem (17-18) is obtained by substituting U in (20).

3.4.1. NUMERICAL TESTS

In this section, we consider an example to show the efficiency and the accuracy of the proposed approach. For $0 < \alpha \leq 1$ and $t \in [0,1]$, we consider the system :

$$\begin{cases} D^{\alpha}\, u(t) = u^{2}(t) + v(t) + \dfrac{\Gamma(\beta+1)}{\Gamma(\beta+1-\alpha)}\, t^{\beta-\alpha} - t^{2\beta} - \sqrt[\gamma]{t} \\ D^{\alpha}\, v(t) = v^{2}(t) + u(t) + \dfrac{\Gamma\left(\frac{\gamma}{2}+1\right)}{\Gamma\left(\frac{\gamma}{2}+1-\alpha\right)}\, t^{\frac{\gamma}{2}-\alpha} - t^{\gamma} - t^{\beta}, \end{cases} \tag{22}$$

such that

$$\begin{cases} u(0) = 0 \\ v(0) = 0. \end{cases} \tag{23}$$

The exact solution of (22) and (23) is given by

$$\begin{cases} u_e(t) = t^{\beta} \\ v_e(t) = \sqrt[\gamma]{t}. \end{cases}$$

We employ the Legende wavelet method combined with the decoupling and quasi-linearization technique for studying the solutions of the problem (22–23).

In the Figure 2, we see the evolution of the logarithmic error induced by the decoupling and quasi-linearization technique defined in (16). We observe a strict decrease of the error, which explains the convergence and the stability of the solution.

Figure 2: Example 2: Error induced by DQLT.

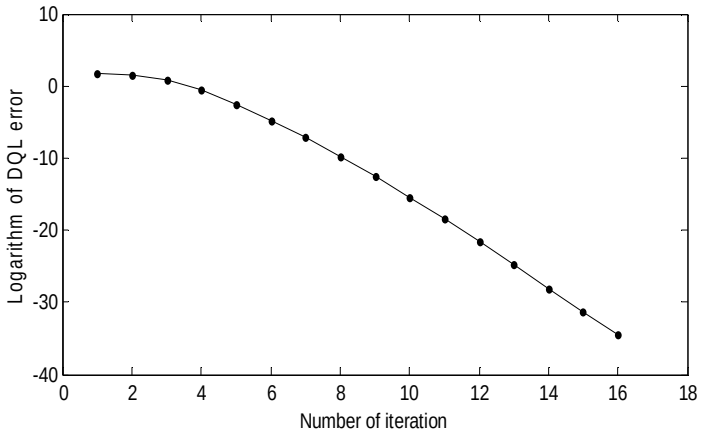

Then, as we know the exact solution, we estimate the absolute error of each solution is produced by cumulate of truncation, LWM and DQL technique by the following formula

$$E_A = \|u - u_e\|_2. \tag{24}$$

Figure 3: Example 2:The analytical and approximate solutions.

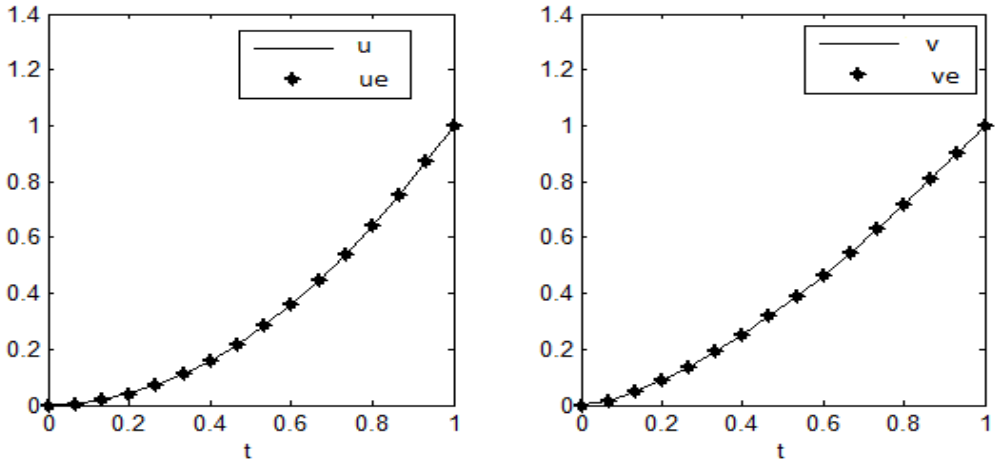

We observe a good agreement between the analytical and approximate solutions (see Figure 3). However, the obtained result shows that this approach can provide better performance.

Table 1: Example 2: The point wise errors for *u*.

t	Exact Solution	j=3 and nc=4	j=3 and nc=8	j=5 and nc=4	j=5 and nc=8
0	0	6.3318e-04	1.5723e-04	3.9868e-05	9.9852e-06
0.2	0.0400	6.4165e-04	1.6826e-04	4.0775e-05	1.0361e-05
0.4	0.1600	5.4928e-04	1.5991e-04	3.8131e-05	1.0120e-05
0.6	0.3600	4.5914e-04	1.4914e-04	3.5756e-05	9.8017e-06
0.8	0.6400	4.4651e-04	1.3749e-04	3.6947e-05	9.4494e-06
1	1.0000	4.5500e-04	1.2532e-04	3.9832e-05	9.0781e-06

Table 2: Example 2: The point wise errors for *v*.

t	Exact Solution	j=3 and nc=4	j=3 and nc=8	j=5 and nc=4	j=5 and nc=8
0	0	7.8510e-04	8.8309e-04	7.5065e-05	1.0596e-04
0.2	0.0894	8.7458e-04	1.9219e-04	7.5034e-05	2.0449e-05
0.4	0.2530	1.7925e-03	3.2299e-04	2.2016e-04	3.9049e-05
0.6	0.4648	1.0542e-03	3.4945e-04	1.1705e-04	4.2348e-05
0.8	0.7155	5.1373e-05	3.7980e-04	1.8159e-04	4.6889e-05
1	1.0000	3.7651e-05	3.8612e-04	1.7892e-04	4.7739e-05

Finally, as can be seen in Tables 1-2, only a small number of collocation points is needed to get the approximate solution, which is a full agreement with the exact solution up to 6 Digits. The obtained solutions show that this approach can effectively solve systems of fractional differential equations.

4. A SIMULATION STUDY

In this section, we propose a new numerical solution for the mathematical model described in Section 2. The proposed approach seems to be very efficient for nonlinear differential systems. Numerical test shows that one important feature of our approach is that it gives a high-quality of the solution as well as a stability and a computational speed for a small number of collocation points.

So, let us consider a small-scale reverse osmosis desalination fractional order model (2), where the co-current flow pattern is treated as shown in figure 1, associated with the conditions:

$$Q_{sw}(0) = 226.8$$
$$\dot{Q}_{ss}(0) = 2\,Q_{sw}(0)$$
$$Q_{fw}(0) = 0$$
$$\dot{Q}_{fs}(0) = 0$$

and

$$\frac{dQ_{sw}}{dx}(0) = \frac{dQ_{sw}}{dx}(0) = \frac{dQ_{sw}}{dx}(0) = \frac{dQ_{sw}}{dx}(0) = 0.$$

The membrane specifications and the operating parameters are given in the table 3 obtained from [29,28].

Table 3: The operating parameters.

Parameters	Value
The membrane diameter (D_m)	0.0576 m
Water density (σ_w)	10^3 kg/m^3
Solute permeability coefficient (B_s)	1.12×10^{-4} m/h
Water permeability constant (A_w)	4.2×10^{-13} h/m
Proportionality coefficient (κ)	$1.02 \times 10^{+12}$ m^2/h^2
Transmembrane pressure (ΔP)	$4.02 \times 10^{+13}$ kg/m/ h^2

The feed rate consisting of water and salts (solute) flows continuously and tangentially inside the membrane. Following the permselectivte property of the membrane, water diffuses faster than the solute. At the output of the module, we obtain a permeate at the tube side with a low concentration of salts, and a retentate at the shell side with a very high concentration of salts (Figure 1).

The results of simulation obtained by the proposed numerical solution method are shown in Figures 4–7. The first finding is that the behavior of the curves predicted by the model are very close to these obtained in the literature.

Figures 4–7 (A) show the variation of the solute and water flow rate in the tube and shell side along the dimensionless parameter *x*. As predicted, the variation of water and solute flow rate are close to zero at the entrance of the module. In reality, at this point of the module, water and solute flow rates are both constants and therefore, their variation is equal to zero. This behavior is demonstrated in the proposed model, which is not the case of the classical model with an integer derivative (see Figures 4–7 (B)).

Figure 4: The flow rate of the solute in tube-side.

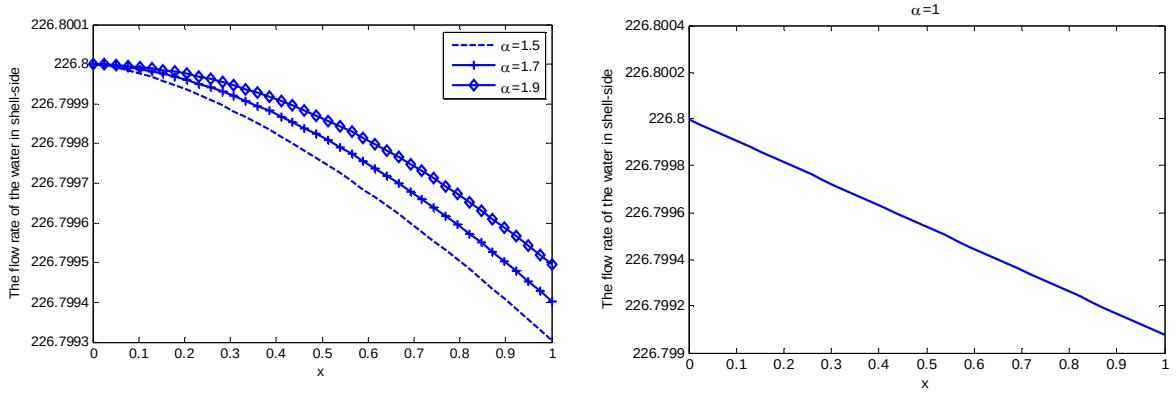

(A) (B)

Figure 5: The flow rate of the water in tube-side.

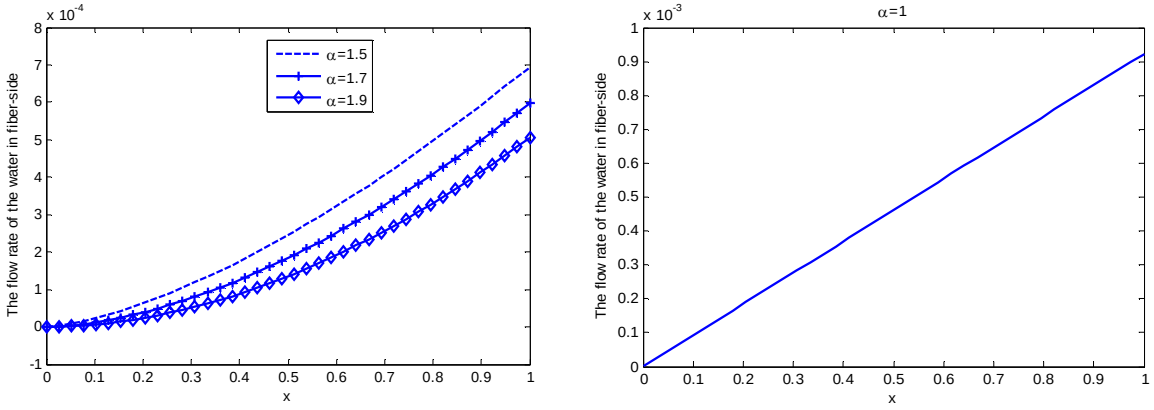

(A) (B)

Figure 6: The flow rate of the solute in shell-side.

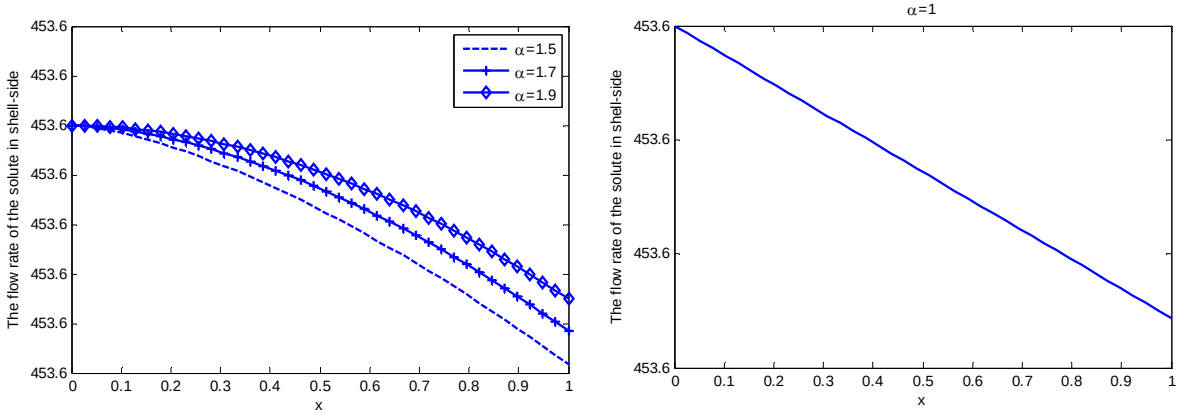

(A) (B)

Figure 7: The flow rate of the water in shell-side.

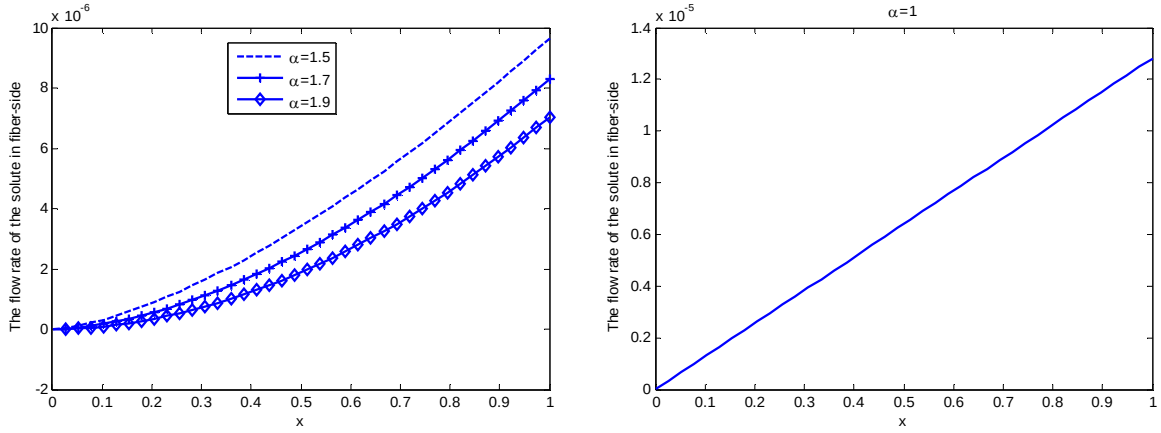

(A) (B)

Another means to verify the accuracy of the obtained results is to establish a matter balance. The following equation expresses the relative mass balance applied to the module:

$$V_1 = \frac{Q_{water}-(Q_{permeate\_water}+Q_{retentate\_water})}{Q_{feed\_water}} = 0,$$

$$V_2 = \frac{Q_{solute}-(Q_{permeate\_solute}+Q_{retentate\_solute})}{Q_{feed\_solute}} = 0.$$

The examination of the mass conservation law is a pertinent factor for the validation of our simulation. The results show the quality of the proposed model for α = 1.5, by looking V_1 for the water parameter is of the order of 2.45e-10 and V_2 for the solute parameter is less than 1.08e-12.

5. CONCLUSION

In this study, simulation of small-scale reverse osmosis desalination problem was conducted using a new fractional model. Numerical method of Legendre wavelets associated with the decoupling and quasi-linearization technique was applied to solve equations of mass transfer. Comparison of model predictions with experimental results in the literature reveals that a reasonable agreement exists between them. Simulation results reveal that fractional model can be considered as a more efficient predictor as compared with classical model. According to the model results, the calculation of the difference between the quantity of matter in the feed-side and the permeate-retentate sides shows the quality of the solutions obtained by the proposed model. It can be concluded from the obtained results that the proposed model in this work can well give the best prediction of reverse osmosis desalination phenomena.

REFERENCES

[1] A. Abbas, Model predictive control of a reverse osmosis desalination unit, *Desalin.* **194** (2006) 268–280.

[2] B. Absar and O. Belhamiti, Modeling and computer simulation of a reverse osmosis desalination plant-case study of Bousfer plant-Algeria, *Desalin. Water Treat.* **51** (2013) 5942–5953.

[3] B. Absar, S. E. M. L. Kadi and O. Belhamiti, Reverse osmosis modeling with the orthogonal collocation on finite element method, *Desalin. Water Treat.* **21** (2010) 23–32.

[4] M. G. Marcovecchio, P. A. Aguirre and N. J. Scenna, Global optimal design of reverse osmosis networks for seawater desalination: modeling and algorithm, *Desalin.* **184** (2005) 259−271.

[5] H. J. Oh, T. M. Hwang and S. Lee, A simplified simulation model of RO systems for seawater desalination, *Desalin.* **238** (2009) 128−139.

[6] N. Ablaoui-Lahmar and O. Belhamiti, Numerical study of convection-reaction-diffusion equation by the Legendre wavelet finite difference method. *Adv. Nonlinear Var. Inequal.* **19** (2016) (2) 94−112.

[7] H. Ali Merina and O. Belhamiti, Simulation Study of Nonlinear Reverse Osmosis Desalination System Using Third and Fourth Chebyshev Wavelet Methods. *MATCH Commun. Math. Comput. Chem.* **75** (2016) 629−652.

[8] A. Atangana and A. A. Secer, Note on fractional order derivatives and table of fractional derivatives of some special functions, *Abstr. Appl. Anal.* **2013** (2013) 1−8.

[9] O. Belhamiti, A new approach to solve a set of nonlinear split boundary value problems, *Commun. Nonlinear Sci. Numer. Simulat.* **17** (2012) 555−565.

[10] M. Caputo, Linear model of dissipation whose Q is almost frequency independent − II, *Geophys. J. R. Astron. Soc.* **13** (1967), 529−539.

[11] M. Du, Z. Wang and H. Hu, Measuring memory with the order of fractional derivative, *Sci. Rep*. **3** (2013) 1−3.

[12] K. Diethelm, A fractional calculus based model for the simulation of an outbreak of dengue fever, *Nonlinear Dyn.* **71** (2013) 613−619.

[13] F. Gorenflo and F. Mainardi, Fractional Calculus: Integral and Differential Equations of Fractional Order, in Fractals and Fractional Calculus in Continuum Mechanics, Series CISM Courses and Lecture Notes, Springer Verlag, Wien, **378** (1997), 223−276.

[14] M. Hamou Maamar and O. Belhamiti, New (0,2) Jacobi multi-wavelets adaptive method for numerical simulation of gas separations using hollow fiber membranes, *Commun. Appl. Nonlinear Anal.* **22** (2015) 3, 61−81.

[15] H. A. Jalab and R. W. Ibrahim, Texture enhancement for medical images based on fractional differential masks, *Discrete Dyn. Nat. Soc.* **2013**, Article ID 618536, (2013), 10 pages.

[16] H. A. Jalab and R. W. Ibrahim, Texture enhancement based on the Savitzky-Golay fractional, differential operator, *Math. Probl. Eng.* **2013**, Article ID 149289, (2013), 8 pages.

[17] A. A. Kilbas and S. A. Marzan, Nonlinear differential equation with the caputo fraction derivative in the space of continuously differentiable functions, *Differ. Equ.* **41** (2005) 84−89.

[18] J. Klafter, S. C. Lim and R. Metzler, *Fractional Dynamics. Recent Advances*, World Scientific, Singapore, (2011).

[19] A. D. Khawajia, I. K. Kutubkhanaha and J. M. Wieb, Advances in seawater desalination technologies. *Desalin.* **221** (2008) 47−69.

[20] K. Hakiki and O. Belhamiti, A dynamical study of fractional order obesity model by a combined Legendre wavelet method, submited, (2016).

[21] V. Lakshmikantham and A. S. Vatsala, Basic theory of fractional differential equations, *Nonlinear Anal.* (2008), 2677−2682.

[22] Y. Q. Liu and J. H. Ma, Exact solutions of a generalized multi-fractional nonlinear diffusion equation in radical symmetry, *Commun. Theor. Phys.* **52** (2009) 857−861.

[23] J. Lu and G. A. Chen, Note on the fractional-order Chen system, *Chaos, Solitons and Fractals* **27** (2006) 685−688.

[24] C. Qing−li, H. Guo and Z. A. Xiu−qiong, Fractional differential approach to low contrast image enhancement, *Int. J. Knowledge Lang. Proces.* **3** (2012) 20−29.

[25] M. Rehman and R. A. Khan, The Legendre wavelet method for solving fractional differential equations, *Commun. Nonlinear Sci. Numer. Simulat.* **16** (2011) 4163−4173.

[26] M. Razzaghi and S. Yousefi, Legendre wavelets direct method for variational problems, *Math. Comput. Simul.* **53** (2000) 185−192.

[27] C. H. Wang, On the generalization of Block Pulse Operational matrices for fractional and operational calculus, *J. Frankin Inst.* **315** (1983) 91−102.

[28] C. S. Slater, Development of a simulation model predicting performance of reverse osmosis batch systems, *Separa. Sci. Techno.* **27** (1992) 1361−1388.

[29] C. S. Slater, J. M. Zielinski, R. G. Wendel and C. G. Uchrin, Modeling of small scale reverse osmosis systems, *Desalin.* **52** (1985) 267−284.

[30] V. M. Starov, J. Smart and D. R. Lloyd, Performance optimization of hollow fiber reverse osmosis membranes, Part I. Development of theory, *J. Membrane Sci.* **103** (1995) 257−270.

[31] J. Smart, V. M. Starov and D.R. Lloyd, Performance optimization of hollow fiber reverse osmosis membranes. Part II. Comparative study of flow configurations, *J. Membrane Sci.* **119** (1996) 117−128.